EPJ Web of Conferences **182**, 02085 (2018) https://doi.org/10.1051/epjconf/201818202085
ICNFP 2017

Heavy ion physics at LHCb

Émilie Maurice[1,a] on behalf of the LHCb collaboration

[1] *LAL, Université Paris-Sud, CNRS/IN2P3, Orsay, France*
also at Laboratoire Leprince-Ringuet, École polytechnique, Palaiseau, France

Abstract.
The LHCb detector, with its excellent momentum resolution and particle identification, is ideally suited for measuring heavy quark hadron and quarkonium production properties. Recent LHCb measurements of charmonium and open charm production in several configurations of proton-nucleus collisions are presented.

1 Introduction

Measurements of charmonium and open charm production provide important information about production processes occurring in proton-nucleus collisions [1]. These processes, called "Cold Nuclear Matter" (CNM) effects, are competing with effects due to deconfinement in high energy heavy ion collisions, such as suppression of charmonium production observed at the SPS [2], RHIC [3] or LHC [4, 5]. They must be precisely quantified in order to disentangle them. The LHCb detector [6, 7], optimized for the study of b and c hadrons, is ideally suited for measuring charmonium and open charm decays. The most important features of the detector for these measurements are: track reconstruction down to very low momentum, precise decay vertex reconstruction and particle identification. The LHCb experiment collected heavy ion data in different conditions.

At the end of 2016, an integrated luminosity $\mathcal{L} = 28$ nb^{-1} of proton-lead collisions (12 nb^{-1} of pPb and 16 nb^{-1} of Pbp) was recorded at a center-of-mass energy per nucleon pair of $\sqrt{s_{NN}} = 8.16$ TeV. These data are used to measure the J/ψ production presented in section 2. In early 2013, LHCb recorded $\mathcal{L} = 1.58$ nb^{-1} of proton-lead collisions (1.06 nb^{-1} of pPb and 0.52 nb^{-1} of Pbp) at a center-of-mass energy of 5.02 TeV. The measurements of D^0 production and the ratio between Λ_c^+ and D^0 productions using this sample are respectively detailed in sections 3 and 4. The last section focuses on the preliminary measurements of J/ψ and D^0 production in the fixed-target configuration, unique at the LHC.

2 J/ψ cross section in pPb and Pbp data

The double differential cross-sections of prompt and non-prompt J/ψ production are measured as functions of the J/ψ transverse momentum and rapidity in the nucleon-nucleon centre-of-mass frame, using 2016 proton-lead collisions at $\sqrt{s_{\rm NN}} = 8.16$ TeV [8].

[a] e-mail: emilie.maurice@llr.in2p3.fr

Since the energy per nucleon in the proton beam is larger than in the lead beam, the LHCb detector covers two different 2 acceptance regions: $1.5 < y* < 4.0$ and $-5.0 < y* < -2.5$, where $y*$ is the rapidity in the centre-of-mass frame of the colliding nucleons, with respect to the proton beam direction. The data samples correspond to an integrated luminosity of $13.6 \pm 0.3 \text{nb}^{-1}$ of pPb collisions and $20.8 \pm 0.5\ \text{nb}^{-1}$ of Pbp collisions.

The J/ψ candidates are selected after online (trigger system) and offline selections. Two muons tracks, with a good-quality track fit, a pseudo-rapidity within $2 < \eta < 5$ and a transverse momentum above 750 MeV/c, are required to form a J/ψ candidate with a good-quality vertex and an invariant mass within 120 MeV/c^2 of the known value of the J/ψ mass. The selected J/ψ mesons are either prompt or originating from b-hadron decays. These two contributions are distinguished by exploiting the pseudo proper decay time distributions, obtained from the J/ψ decay vertex position and the primary vertex position. The yields of J/ψ signal candidates, for the prompt and J/ψ from-b-hadrons categories, are determined from a simultaneous two-dimensional fit to their invariant mass and pseudo proper decay time distributions, performed independently in $(p_T, y*)$ bin.

The yields of J/ψ signal candidates are then corrected by the total detection efficiency, defined as the product of the geometrical acceptance and the efficiencies for charged track reconstruction, particle identification, candidate and trigger selections. Except from the particle identification efficiency, which is determined in a data-driven approach, the other efficiencies are evaluated using simulated samples. The charged-track reconstruction efficiency is computed using the simulation, then is corrected using a data-driven tag-and-probe approach. The total detection efficiency is computed in each $(p_T, y*)$ bin.

The measurement of the double-differential production cross-sections of J/ψ mesons is performed as a function of p_T and $y*$ in the ranges $0 < p_T < 14$ GeV/c and $1.5 < y* < 4.0$ for pPb and $-5.0 < y* < -2.5$ for Pbp. The main systematic uncertainties on these measurements are due to the simulation statistics, muon identification, tracking and hardware trigger efficiencies. Nuclear effects are then quantified by the nuclear modification factor, R_{pPb}:

$$R_{pPb}(p_T, y*) = \frac{1}{A} \frac{d^2\sigma_{pPb}(p_T, y*)/dp_T dy*}{d^2\sigma_{pp}(p_T, y*)/dp_T dy*},$$

where $A = 208$ is the mass number of the Pb ion, $d^2\sigma_{pPb}(p_T, y*)/dp_T dy*$ is the J/ψ production cross-section in pPb or Pbp collisions and $d^2\sigma_{pp}(p_T, y*)/dp_T dy*$ is the J/ψ reference production cross-section in pp collisions at the same nucleon-nucleon centre-of-mass energy. The nuclear modification factors for prompt J/ψ and J/ψ-from-b-hadrons production as functions of p_T or $y*$, integrating over the other variable, are shown in Figs. 1.

At forward rapidity, a strong suppression of up to 50% is observed in the case of prompt J/ψ production at low p_T. This behaviour results in a strong suppression in the nuclear modification factor as a function of rapidity shown in Fig 2, where the results at $\sqrt{s_{NN}} = 5$ TeV [9] are also presented and are in good agreement with the new and more precise results at $\sqrt{s_{NN}} = 8.16$TeV.

With increasing p_T, R_{pPb} approaches unity and the suppression is stronger at more forward rapidities. The production of J/ψ-from-b-hadrons is also suppressed compared to that in pp collisions at forward rapidities, as shown in Fig. 2. No dependence as a function of rapidity is observed within the experimental uncertainties. The dependence as a function of the transverse momentum is weaker for J/ψ-from-b-hadrons compared to prompt J/ψ, see Fig. 3, but the nuclear modification factor is also close to unity at high transverse momentum.

At backward rapidity, a weaker suppression of prompt J/ψ production at low p_T is observed, of up to 25%. The nuclear modification factor of J/ψ from b-hadrons at backward rapidity is consistent with unity over the full kinematic region.

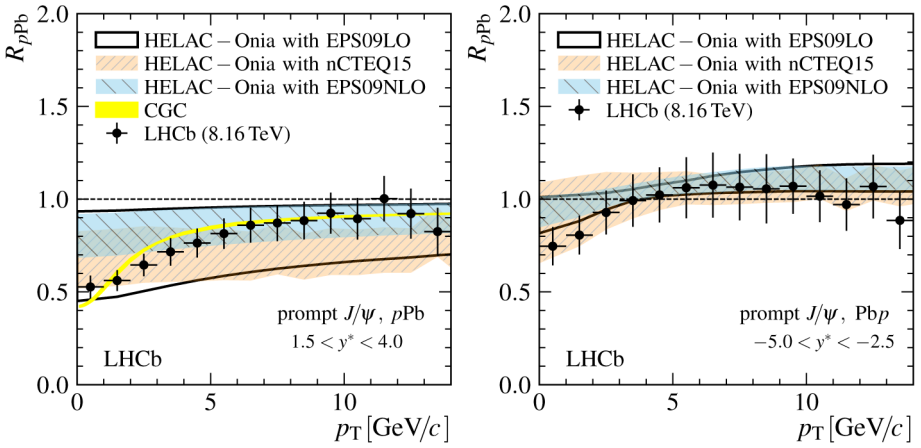

Figure 1. Nuclear modification factor integrated over $y*$ for prompt J/ψ in pPb (left) and Pbp (right).

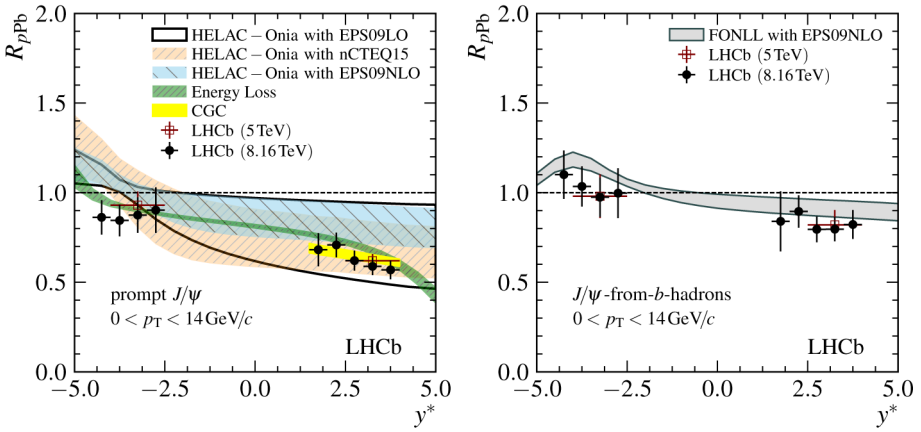

Figure 2. Nuclear modification factor integrated over p_T for prompt J/ψ (left) and J/ψ-from-b-hadrons (right).

These measurements of prompt J/ψ are compared with LHCb 5 TeV result [9] and with theoretical calculations: collinear factorisation using different nuclear parton distribution functions (nPDF) [10, 11] (labelled "HELAC-Onia with EPS09LO", "HELAC-Onia with nCTEQ15" and "HELAC-Onia with EPS09NLO"), Color Glass Condensate effective field theory [12, 13] (labelled "CGC") and coherent energy loss [14] (labelled "Energy Loss"). The measurements of J/ψ-from-b-hadrons nuclear modification factors are compared with a perturbative QCD calculation at fixed-order next-to-leading-logarithms (FONLL) [15, 16] coupled with the EPS09 nPDF set at next-to-leading order [17] (labelled "FONLL with EPS09NLO").

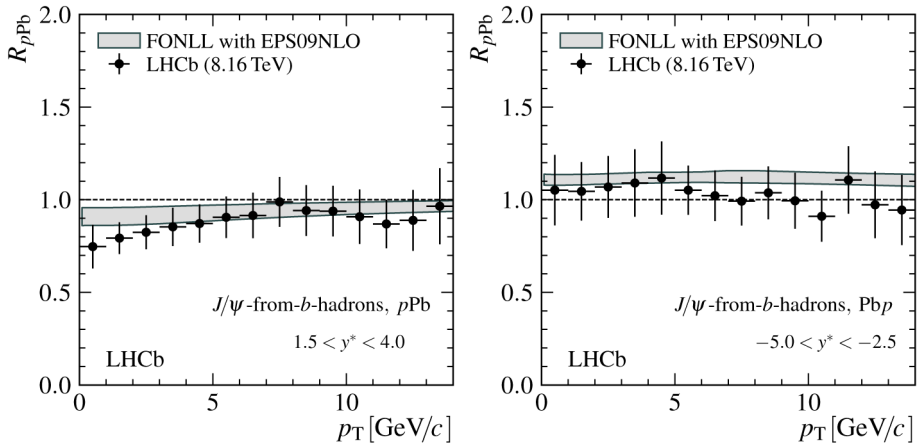

Figure 3. Nuclear modification factor integrated over $y*$ for J/ψ-from-b-hadrons in pPb (left) and Pbp (right).

3 D^0 cross section in pPb and Pbp data

The D^0 cross section measurement was performed using the 2013 proton-lead run, with $\sqrt{s_{NN}} = 5$ TeV [18]. A total integrated luminosity of 1.6 nb^{-1} was recorded, 1.1 nb^{-1} in the pPb configuration and 0.5 nb^{-1} in the Pbp configuration. D^0 candidates are reconstructed in the decay mode $D^0 \to K^-\pi^+$, using tight particle identification criteria based on the RICH detectors. Only prompt D^0 are considered, the D^0 coming from-b-hadron decays are rejected based on their impact parameter with respect to the collision vertex. The numbers of signal candidates are extracted from a fit to their invariant mass distributions and are corrected by the total detection and reconstruction efficiencies computed from detailed Monte Carlo simulation.

Fig 4 shows the single-differential cross-sections as a function of p_T (left) and $y*$ (right), integrated over the other variable. On these two figures, a comparison with the HELAC-Onia tool [19] is shown. This generator is tuned to reproduce measurements performed in pp collisions and is used with different nuclear parton distribution functions (nPDF): EPS09LO, EPS09NLO [17] and nCTEQ15 [22].

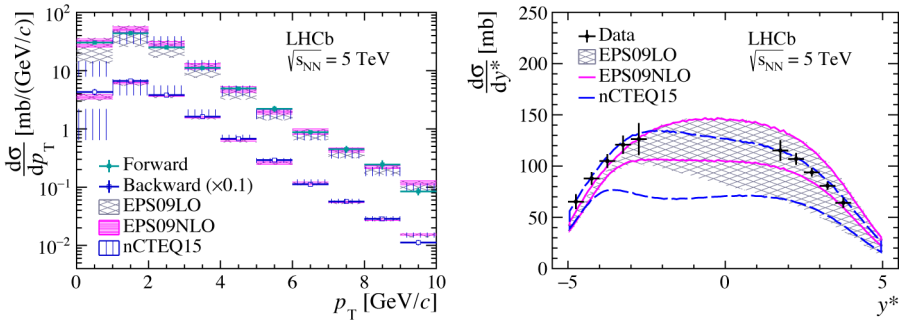

Figure 4. Differential cross-section of prompt D^0 meson production in pPb collisions as a function of (left) p_T ($d\sigma dp_T$) and (right) $y*$ ($d\sigma dy*$) in the forward and backward collision samples.

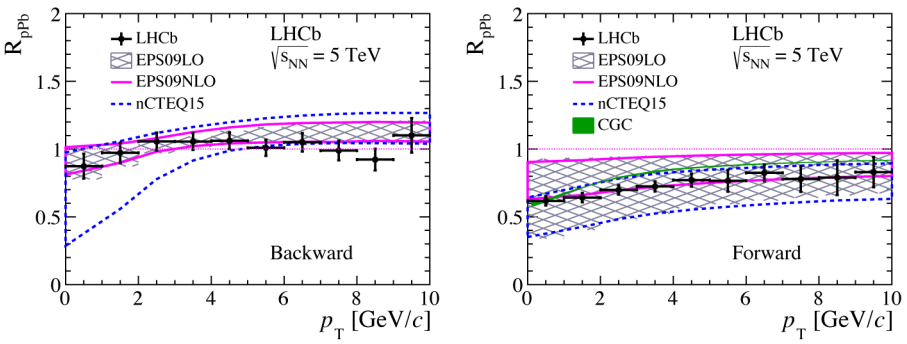

Figure 5. Nuclear modification factor R_{pPb} as a function of p_T for prompt D^0 meson production in the (left) backward data and (right) forward data, integrated over the common rapidity range $2.5 < |y*| < 4.0$ for $p_T < 6$ GeV/c and over $2.5 < |y*| < 3.5$ for $6 < p_T < 10$ GeV/c.

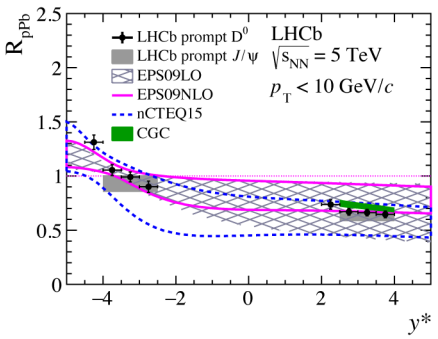

Figure 6. Nuclear modification factor R_{pPb} as a function of $y*$ for prompt D^0 meson production, integrated up to $p_T = 10$ GeV/c.

CNM effects are studied comparing the production cross-sections in proton-lead collisions with the ones in proton-proton collisions at the same energy. The measurement of the prompt D^0 reference cross-section in pp at $\sqrt{s_{NN}} = 5$ TeV was performed using the data collected in 2015 [15] when $\mathcal{L} = 8.6$ pb^{-1} of pp collisions were recorded during a dedicated LHC run at this energy. Figures 5 and 6 show the results as a function of p_T and y* for R_{pPb} respectively. On these figures are superimposed theoretical predictions using various models for the description of CNM. HELAC-Onia is used to illustrate the shadowing and anti-shadowing effects due to the modification of the gluon density functions inside the lead nucleons compared to protons, parametrized with various nPDFs sets (EPS09LO, EPS09NLO and nCTEQ15). The Color Glass Condensate model computations [16] are also compared with the experimental measurements. On these plots, a significant suppression of D^0 production in proton-lead collisions compared to pp collisions can be observed, at low p_T in the forward region (positive rapidities). This effect is reproduced by the theoretical models within large uncertainties.

4 Λ_c^+/D^0 ratio in pPb and Pbp data

The differential production cross-sections of Λ_c^+ baryons are measured in the 2013 proton-lead collisions [23], the same data sample used for the D^0 cross section measurement. The Λ_c^+ production measurement is performed as a function of its transverse momentum and rapidity in the kinematic range $2 < p_T < 10$ GeV/c and $1.5 < y* < 4.0$ for the forward sample and $-4.5 < y* < -2.5$ for the backward sample. The prompt Λ_c^+ signal is reconstructed through the decay: $\Lambda_c^+ \to pK^-\pi^+$. The number of inclusive Λ_c^+ candidates is determined with a fit to the invariant mass distribution, then the prompt component is distinguished from the Λ_c^+ coming from b-hadron decays using the impact parameter with respect to the collision vertex. The number of Λ_c^+ candidates and the efficiency are estimated independently for each p_T and $y*$ bin.

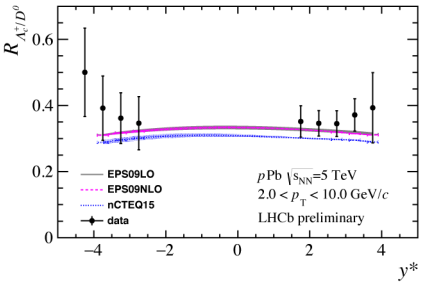

Figure 7. Production ratio between Λ_c^+ baryons and D^0 mesons as a function of $y*$ integrated over $2 < p_T < 10$ GeV/c.

The baryon-to-meson cross-sections ratio $\sigma_{\Lambda_c^+}/\sigma_{D^0}$ is computed as the ratio of cross-sections of Λ_c^+ and D^0 production. This ratio integrated over p_T is presented in Fig 7.

5 Fixed-target physics

LHCb provides the unique opportunity at the LHC to operate in a fixed target mode, thanks to the System for Measuring Overlap with Gas (SMOG). Originally designed for precise luminosity measurements [2], SMOG allows to inject noble gas such as argon or helium inside the primary LHC vacuum around the LHCb vertex detector (VELO). Since 2015, LHCb has started to exploit SMOG to collect data for physics analysis, with different beam and target configurations, allowing unique production studies which are relevant to cosmic ray and heavy ions physics [24].

The first analysis of heavy-flavour production measured by the LHCb experiment in a fixed-target mode is presented: J/ψ and D^0 production processes in proton-Argon sample at $\sqrt{s_{NN}} = 110.4$ GeV.

The study reported here uses a data sample of pAr collisions of a proton beam (with a momentum of 6.5 TeV/c) with the argon gaseous target. The analysis studies the J/ψ and D^0 candidates reconstructed in $J/\psi \to \mu^+\mu^-$ and $D^0 \to K^-\pi^+$ decays. In order to fully benefit from the LHCb detector's performance, only events with a primary vertex reconstructed between -200 and 200 mm with respect to the nominal interaction point are considered. The numbers of J/ψ and D^0 signal candidates are extracted from unbinned maximum likelihood fits to their mass distributions, as shown in Fig 8 covering the full rapidity and transverse momentum ranges. For differential studies, the number of signal candidates is determined independently as a function of their transverse momentum p_T and rapidity y.

The yields determined from the mass fit are corrected for event trigger and selection efficiencies, including primary vertex and particle reconstruction, geometrical acceptance of the detector and particle identification. Except for particle identification and tracking efficiencies that are obtained based on pp data, all the efficiencies are determined from fully simulated pAr events.

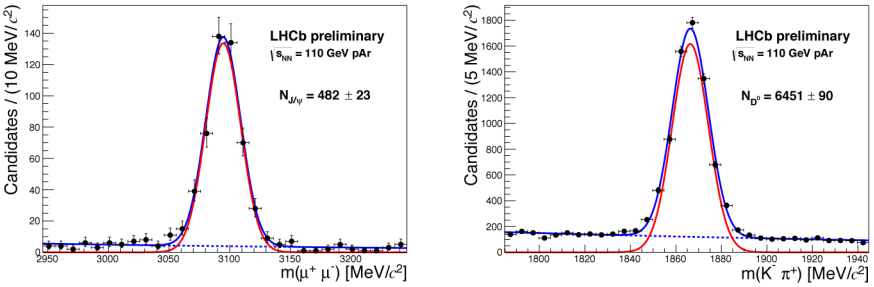

Figure 8. (left) $J/\psi \to \mu^+\mu^-$ and (right) $D^0 \to K^-\pi^+$ mass distributions with the fit functions compared. The black points are the data, the red line the signal, the dashed blue line the background, and the solid blue the sum of background and signal.

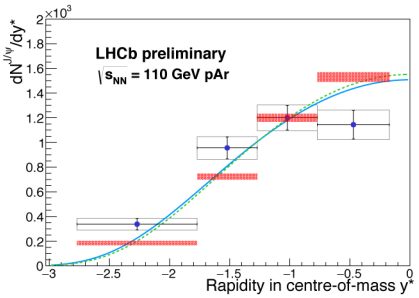

Figure 9. Differential $J/\psi \to \mu^+\mu^-$ corrected yields, as a function of $y*$. Red boxes correspond to Pythia [20]. Blue and green curves correspond to two phenomenological parametrizations based on Ref. [21]. The data points indicate the centres of the bins.

Several systematic uncertainties affect either the determination of the number of signal events or the computation of the efficiencies. They are computed in every rapidity and transverse momentum interval. The most important systematic uncertainties come from the differences between pAr and pp track multiplicity for the efficiency estimate, from the contamination of residual pp collisions, from the signal and background modelling, and from the neglected non-prompt contribution of J/ψ and D^0. Fig. 9 presents J/ψ mesons corrected yields as a function of the rapidity in the centre-of-mass system of the nucleon-nucleon collision, $y*$ (given by: $y* = y - 4.77$, where 4.77 is the rapidity of the centre-of-mass in the LHCb frame at 110.4 GeV) and transverse momentum compared to phenomenological parametrizations based on Ref [13].

6 Conclusions and prospects

LHCb is well-suited to measure Cold Nuclear Effects in proton-nucleus collisions. Measurements of D^0 and Λ_c^+ production were obtained analysing the proton-lead collisions recorded at LHCb in 2013. The largest sample of proton-lead collisions collected by LHCb in 2016 was used to measure the J/ψ production. These measurements are in good agreement with the theoretical calculations. On top of that, LHCb has started its heavy-flavour production measurement in its fixed-target configuration with the measurement of J/ψ and D^0 yields. This study will be completed by the analysis of the pHe collisions collected in 2016 and pNe collisions to be taken in November 2017.

References

[1] A. Andronic et al., Eur. Phys. J.C **76** (2016) 107, arXiv:1506.03981
[2] NA50 collaboration, M. C. Abreu et al., Phys. Lett. B **410** (1997) 327
[3] PHENIX collaboration, A. Adare et al., Phys. Rev. Lett. **98** (2007) 232301
[4] ALICE collaboration, B. Abelev et al., Phys. Rev. Lett. **109** (2012) 072301, arXiv:1202.1383
[5] CMS collaboration, V. Khachatryan et al, Eur. Phys. J. C **77** (2017) 252, arXiv:1610.00613
[6] LHCb collaboration, A. A. Alves Jr et al., JINST **3** (2008) S08005
[7] LHCb Collaboration, R. Aaij et al., Int. J. Mod. Phys. A **30** (2015) 1530022, arXiv:1412.6352
[8] LHCb Collaboration, R. Aaij et al., Phys. Lett. **B774** (2017), arXiv:1706.07122
[9] LHCb collaboration, R. Aaij et al., JHEP **02** (2014) 072, arXiv:1308.6729
[10] H.-S. Shao, Comput. Phys. Commun. **184** (2013) 2562, arXiv:1212.5293
[11] H.-S. Shao, Comput. Phys. Commun. **198** (2016) 238, arXiv:1507.03435
[12] B. Ducloué et al., Phys. Rev. **D91** (2015) 114005, arXiv:1503.02789
[13] B. Ducloué et al., Phys. Rev. **D94** (2016) 074031, arXiv:1605.05680
[14] F. Arleo et al., JHEP **03** (2013) 122, arXiv:1212.0434
[15] M. Cacciari et al., JHEP **05** (1998) 007, arXiv:hep-ph/9803400
[16] M. Cacciari et al., JHEP **03** (2001) 006, arXiv:hep-ph/0102134
[17] K. J. Eskola et al., JHEP **04** (2009) 065, arXiv:0902.4154
[18] LHCb Collaboration, R. Aaij et al., JHEP **10** (2017) 090, arXiv:1707.02750
[19] J. P. Lansberg et al., Eur. Phys. J. C **77** (2017) 1, arXiv:1610.05382
[20] T. Sjostrand et al., Comput. Phys. Commun. **178** (2008) 852, arXiv:0710.3820
[21] F. Arleo et al., JHEP **05** (2013) 155, arXiv:1304.0901
[22] K. Kovarik et al., Phys. Rev. D **93** (2016) 085037, arXiv:1509.00792
[23] LHCb Collaboration, R. Aaij et al., LHCb-CONF-2017-005
[24] LHCb Collaboration, R. Aaij et al., LHCb-CONF-2017-001